TISSUE ENGINEERING: Part C
Volume 17, Number 4, 2011

DOI: 10.1089/ten.tec.2010.0368

Noninvasive Multimodal Evaluation of Bioengineered Cartilage Constructs Combining Time-Resolved Fluorescence and Ultrasound Imaging

Brett Z. Fite, B.S.,[1,2] Martin Decaris, B.S.,[1] Yinghua Sun, Ph.D.,[1] Yang Sun, Ph.D.,[1] Adrian Lam, B.S.,[1] Clark K.L. Ho, B.S.,[1] J. Kent Leach, Ph.D.,[1] and Laura Marcu, Ph.D.[1]

A multimodal diagnostic system that integrates time-resolved fluorescence spectroscopy, fluorescence lifetime imaging microscopy, and ultrasound backscatter microscopy is evaluated here as a potential tool for assessing changes in engineered tissue composition and microstructure nondestructively and noninvasively. The development of techniques capable of monitoring the quality of engineered tissue, determined by extracellular matrix (ECM) content, before implantation would alleviate the need for destructive assays over multiple time points and advance the widespread development and clinical application of engineered tissues. Using a prototype system combining time-resolved fluorescence spectroscopy, FLIM, and UBM, we measured changes in ECM content occurring during chondrogenic differentiation of equine adipose stem cells on 3D biodegradable matrices. The optical and ultrasound results were validated against those acquired via conventional techniques, including collagen II immunohistochemistry, picrosirius red staining, and measurement of construct stiffness. Current results confirm the ability of this multimodal approach to follow the progression of tissue maturation along the chondrogenic lineage by monitoring ECM production (namely, collagen type II) and by detecting resulting changes in mechanical properties of tissue constructs. Although this study was directed toward monitoring chondrogenic tissue maturation, these data demonstrate the feasibility of this approach for multiple applications toward engineering other tissues, including bone and vascular grafts.

Introduction

The engineering and growth of functional tissues in the laboratory setting is a promising approach to address the significant shortage of transplantable tissues.[1,2] The quality of the tissue construct must be evaluated at multiple points during culture to assess cell phenotype, extracellular matrix (ECM) content, and mechanical properties, all of which contribute to the functionality of the construct. However, current evaluation methods are destructive and reduce the amount of graft material for implantation.[3,4] Hence, there remains a significant need for nondestructive techniques to reliably assess the presence of known ECM macromolecules characteristic of the tissue and their resultant contribution to tissue quality to advance the field of tissue engineering for clinical use.

Optical and ultrasound techniques are of particular interest for characterizing growing tissues due to their capacity to probe composition and structure in a nondestructive and noninvasive manner. Optical methods based on fluorescence lifetime contrast such as time-resolved fluorescence spectroscopy (TRFS) and fluorescence lifetime imaging microscopy (FLIM) can detect biochemical and physiological transformations in tissue[5] and are known to improve the specificity of fluorescence measurements.[6–8] Several endogenous biomolecules, including structural proteins (e.g., collagen and elastin) and enzyme cofactors (e.g., NADH and FAD), are responsible for tissue autofluorescence.[9] Changes in the fluorescence properties of tissue are reflective of native fluorophore deposition and, thus, the relative contribution and distribution of individual fluorophores within the tissue. Tissue autofluorescence has been previously utilized to detect pathologic and physiologic tissue changes in both clinical and research settings.[10,11] Moreover, TRFS effectively monitored differentiation of human adipose stem cells (ASCs) along the osteogenic lineage *in vitro* in 2D culture.[12] TRFS provides emission information (both intensity and time-resolved) that can characterize tissues of a given lineage, yet does not provide spatial distribution of tissue fluorophores. FLIM enables recording of large amounts of lifetime information in an image format, and can be combined in a number of ways with emission spectroscopy. One advantage of FLIM is its ability to easily detect heterogeneity within a given sample. In combination, TRFS and FLIM can

[1]Department of Biomedical Engineering and [2]Biophysics Graduate Group, University of California, Davis, California.

provide complimentary information, which may characterize a biological sample through the determination of the identity, quantity, and distribution of ECM content. Ultrasound backscatter microscopy (UBM) can provide additional structural information that can be correlated to tissue microstructure as well as stiffness, a primary endpoint for the functionality of bioengineered connective tissues such as cartilage and bone. UBM offers significantly greater penetration depth (up to 6 mm) than either FLIM or TRFS. Additionally, mechanical properties, which are critical to and correlate with the functionality of the tissue,[13–15] can be discerned from UBM data.

Mature cartilage possesses a low cellularity and is composed primarily of ECM and water (~80%).[16] The generation of cartilage constructs derived from autologous chondrocytes, autologous or allogenic multipotent mesenchymal stem cells,[17,18] embryonic stem cells, and other cell sources[19–21] is an exciting alternative to current treatment strategies. Cartilage ECM consists primarily of collagen, especially collagen type II, and proteoglycans in the form of hydrated glycosaminoglycans (GAGs), which provide mechanical integrity to the tissue.[22] When in its mature form, collagen is highly cross-linked[23] and exhibits a structured orientation of these cross-links.[22,24] Collagen autofluorescence originates from the formation of cross-links between the fibrils,[25] thereby providing a measure of the collagen maturity that may offer an indirect measure of the mechanical strength of the tissue construct.

We hypothesized that a multimodal approach combining optical and ultrasonic methods (TRFS, FLIM, and UBM) could be used to assess changes in ECM deposition resulting from the chondrogenic differentiation of equine ASCs (eASCs) on 3D biodegradable matrices. The goals of this study were to test the hypothesis that TRFS, FLIM, and UBM can be utilized to monitor changes in ECM deposition and content over time and to correlate these data with the mechanical properties of the construct.

Materials and Methods

Cell culture

eASCs were isolated as previously described[26,27] and expanded in Dulbecco's modified Eagle's medium F-12 (Invitrogen, Carlsbad, CA) supplemented with 10% fetal bovine serum (JR Scientific, Woodland, CA), 1% penicillin/streptomycin, and 0.1% amphotericin β (Mediatech, Mannassas, VA). Cells were maintained in standard CO_2 incubators at 37°C and passaged at 80%–90% confluency before experimentation. All experiments were performed with cells at passage 3.

Scaffold fabrication, cell seeding, and construct culture

Scaffolds were prepared from poly(lactide-co-glycolide) using a gas foaming/particulate leaching method as previously described.[28] Scaffolds (8.5 mm diameter × 1.5 mm thickness) were sterilized with 95% ethanol for 30 min, and eASCs were statically seeded at 1×10^6 cells per scaffold in 70 μL of a 50:50 mixture of growth media and growth factor-reduced Matrigel (BD Biosciences, San Jose, CA). After adhesion for 90 min, scaffolds were moved to 12-well culture dishes containing 2 mL of media per well for 24 h. The medium was refreshed with maintenance media or commercial chondrogenic media (Zen-Bio, Raleigh, NC), with scaffolds cultured in maintenance media serving as the control group. Scaffolds were placed on an XYZ shaker, agitated at 25 rpm in standard culture conditions (37°C, 5% CO_2, 95% air), and maintained for up to 7 weeks, with medium changes occurring three times per week.

TRFS measurements

ECM and collagen composition within tissue constructs were interrogated using a TRFS prototype apparatus developed in our lab and detailed elsewhere.[12] In brief, a pulsed nitrogen laser (337 nm; 0.7 ns; 30 Hz) provided the excitation light through an optical fiber (600 μm core diameter, NA = 0.22), which was positioned perpendicular to the sample and directed light onto the sample. Sample autofluorescence was collected via a collection fiber and dispersed by a spectrophotometer after which scattered excitation light was removed by the use of a long pass filter (340 nm). The fluorescence signal was detected via a gated multichannel plate photomultiplier tube amplified by a wideband preamplifier (1.5 GHz), captured by a fast digitizer (2.5 GHz bandwidth, 20 G samples/s), and transferred to a computer utilizing custom analytical software written in LabVIEW. The fluorescence emission of each sample was obtained by scanning of the monochromator across a spectral range of 360–560 nm (steps of 5 nm, scanning time: 25 s) and by integration of the measured fluorescence pulse transients over time. The laser output power was adjusted to 2 μJ/pulse (measured at the end of the optical fiber), which yielded a maximum fluence of 707 $\mu J/cm^2$ per pulse at the tissue surface. Measurements were taken from three points on the sample, with the probe placed in direct contact with the sample. The fluorescence spectra were then normalized by dividing the fluorescence intensity at each measured emission wavelength by the peak intensity. Reflected laser pulses from the sample were measured and used to represent the temporal profile of the laser pulse. This profile was used in the Laguerre polynomial deconvolution technique to estimate the intrinsic fluorescence decay and to calculate the fluorescence lifetime as previously reported.[29,30] The average fluorescence lifetime was computed as the interpolated time at which the deconvolved fluorescence decayed to $1/e$ of its maximum value. Four Laguerre coefficients (LEC-0, LEC-1, LEC-2, and LEC-3) obtained during the process of the deconvolution were also used for differentiation of the tissue composition. The steady-state spectrum was calculated by integrating the fluorescence decay as a function of time at each wavelength over the whole emission range. Control values were obtained by averaging all measurements of control samples for all time points since no significant change was observed for control samples at any time point.

FLIM measurements

The FLIM system consisted of a gated intensified camera (ICCD) 4 Picos, a pulsed nitrogen laser, an imaging bundle with a gradient index (GRIN) lens objective, and a filter wheel as described previously.[31] Similar to TRFS measurements, the sample was excited with a pulsed nitrogen laser (337 nm, 0.7 ns pulse width). A maximum fluence of 0.80 $\mu J/cm^2$ per pulse was delivered at the tissue surface. The

excitation light was delivered via a high numerical aperture (0.4) 200 μm core diameter polymer fiber. The fluorescence light was collected using the GRIN lens objective (NA of 0.5, 0.5 mm diameter, 4 mm field of view) cemented to a fiber image guide (0.6 mm diameter, 10,000 fibers). The excitation optical fiber and the image guide were integrated into an imaging probe of 2 mm outer diameter. A 20× objective magnified the fluorescence image to cover the ICCD sensor. A filter wheel inserted after the objective facilitated the selection of the two emission wavelength bands of interest (377 ± 25 nm and 460 ± 30 nm). Subsequently, the image was recorded by the ICCD with 0.5 ns gating time (image acquisition time: 1.5 min). A graphical-user-interface composed in MATLAB was utilized for image processing and lifetime deconvolution. The Laguerre polynomial deconvolution technique was also utilized for rapid deconvolution of the time-dependent fluorescence images as previously described.[29] Mean fluorescence lifetimes for samples cultured up to 7 weeks were determined by averaging all pixels from all FLIM images for a given sample type and time point. As FLIM measures average fluorescence lifetime at each pixel in the image, mean fluorescence lifetime is the statistical mean of multiple average fluorescence lifetime values. Average fluorescence lifetime refers to the interpolated time for fluorescence intensity to decay $1/e$ of its maximum (given that more than a single fluorophore contributes to the lifetime value observed).

UBM measurements

The UBM experimental setup was previously described.[32] Briefly, a high-voltage pulser generating a rectangular wave (200 V peak-to-peak) was used to drive the transducer. The received radiofrequency (RF) echoes were amplified with a 30 dB low-noise amplifier and filtered with a bandpass filter (24–90 MHz). A 12 bit analog-to-digital converter with a sampling rate of 400 M samples/s was employed, which maintained the signal-to-noise ratio of the received RF signals and provided good resolution and dynamic range of 60 dB. A custom-built positioning assembly incorporating a miniature precision linear motorized stage (1 μm resolution) allowed for scanning and forming an image.[32] A customized 40 MHz focused transducer (aperture size of 3.75 mm, 63% bandwidth, 6 mm focal depth) was used (Ultrasonic Transducer Resource Center, University of Southern California, Los Angeles, CA). The axial and lateral resolution (30 and 65 μm, respectively) was estimated from the image acquired by scanning across a 13 μm tungsten wire (subresolution point target). UBM data acquisition and analysis was accomplished via customized LabVIEW and MATLAB scripts, respectively. To form an ultrasound image, DC offset was first subtracted from the RF data, and the band-pass filter with proper frequency range was used to remove the noise. The Hilbert transform was applied to the filtered RF signals to detect the envelopes, followed by logarithmical compression to display the images with a wide dynamic range. Then, the processed data for each line of sight were displayed as a gray-scale B-mode ultrasound image showing the reconstruction of the cross section of the tissue constructs. In an effort to noninvasively explore construct mechanical features, attenuation of the UBM RF signal was quantified over a region of interest of 2 mm lateral (100 pulses) and 1.2 mm in depth. Each line scan was taken in 1 s. The UBM data were processed as follows: First, the ultrasound RF signals were averaged over the 100 pulses within the image and then averaged over the samples. Second, the envelop of the mean RF signal was detected and the RF data were logarithmically compressed. Third, the intensity of the envelop of ultrasound signals was normalized by the maximum value and plotted as a function of depth. The integrated area below the RF profile was quantified and used as an indicator for the signal attenuation, which was then averaged within the region of interest. Attenuation was compared for each type of tissue constructs as a function of culture time.

DNA quantification

Scaffolds were bisected and collected at weeks 1, 3, 5, and 7, rinsed in phosphate-buffered saline (PBS), minced with a razor blade, and placed in 200 μL of passive lysis buffer (Promega, Madison, WI). The buffer was sonicated for 3 s followed by centrifugation for 5 min at 10,000 rpm. The supernatant was removed, and total DNA content was determined using the Quant-iT PicoGreen dsDNA kit (Invitrogen).[33]

Compressive testing of cell-seeded scaffolds

Scaffolds from each time point were rinsed in PBS and placed in an Instron 3345 compressive testing device as described.[28] Scaffolds were loaded between two unconfined, impermeable flat platens and compressed at 1 mm/min. Compressive modulus of the samples was calculated from the linear portion of the force–displacement graph for strain ranging from 0% to 20%.

Histological staining

Bisected scaffolds collected at each time point ($n = 2$) were rinsed in PBS, fixed in 10% formalin overnight, and stored in 70% ethanol. Scaffolds were then encased in HistoGel (ThermoFisher Scientific, Kalamazoo, MI) before paraffin embedding and sectioning, a process that dissolves most of the polymer scaffold. Cell morphology was observed from hemotoxylin and eosin staining of scaffold sections. Collagen deposition was detected by staining with picrosirius red (PSR), whereas the presence of proteoglycans was observed by staining with Safranin-O with counterstaining by Fast Green (FCF) solution (both from Sigma Aldrich, St. Louis, MO) using standard protocols.

Collagen content and fiber color

Collagen fiber orientation was observed by imaging PSR-stained samples at 100× magnification on a microscope set up for circularly polarized light imaging. After capturing multiple fields of view from each slide, collagen content was calculated as a percentage of the area of each image (expressed in pixels) utilizing a custom MATLAB script that analyzed each pixel within a given image.

Collagen II immunohistochemistry

Paraffin-embedded sections were deparaffinized and rehydrated. Tissue sections were pretreated with proteinase K for antigen retrieval, and endogenous peroxidase activity

was quenched with 3% H_2O_2 in water. Sections were blocked with goat serum for 30 min, followed by incubation with mouse monoclonal antibody CIIC1 (Developmental Hybridoma Studies Bank, University of Iowa) diluted at 1:2.5 overnight at 4°C. This antibody has been reported to cross-react against equine collagen type II.[17] After rinsing, slides were successively incubated with a biotinylated secondary goat anti-mouse IgG antibody, streptavidin-HRP, DAB chromogen, and counterstained with Weigert's hematoxylin (Sigma). Equine medial femoral condyle tissue was processed in parallel to verify specificity of the primary antibody, whereas sections treated with PBS (no primary antibody) were used as a negative control. Positive staining is indicated by the presence of brown staining on the tissue sections.

Data analysis and statistics

Data are presented as mean and standard error of the mean from at least four independent measurements. Statistical significance was established via a two-way ANOVA analysis of control samples, chondrogenic samples, and time point implemented in a parametric test with the exception of the UBM results, which utilized a Student's *t*-test. Statistical significance was established at $p < 0.05$.

Results

Time-resolved fluorescence spectroscopy

Fluorescence emission spectra (Fig. 1A) of cells induced toward the chondrogenic lineage exhibited broad emission with a peak at ~430–440 nm in control samples, weeks 1 and 3 samples, and the peak was slightly blue-shifted at ~410–420 nm in week 5 and 7 samples. These wavelengths were chosen to provide high signal-to-noise ratio while remaining within a range where changes in collagen cross-links can be observed. A marked and statistically significant increase in overall fluorescence intensity of the chondrogenic spectra was observed throughout the study duration, suggesting an increase in the amount of autofluorescent molecular species in tissue constructs. Fluorescence emission was further characterized by an increase of the average radiative fluorescence lifetime values as a function of time from week 1 (1.19 ± 0.05 ns) to week 7 (2.18 ± 0.14 ns), suggesting the formation of a new fluorescent component during culture. For all wavelength ranges, chondrogenic samples from weeks 5 and 7 exhibited a significant increase in average fluorescence lifetime values over control samples (Fig. 1B). However, the increase in radiative lifetime for chondrogenic samples was more pronounced at longer wavelengths, with the greatest increase measured within 480–530 nm. The Laguerre coefficients retrieved through numerical deconvolution also demonstrated a change in the fluorescence decay dynamics during the chondrogenic differentiation process (data not shown).

Fluorescence lifetime imaging microscopy

Differences in fluorescence lifetimes for cell-seeded scaffolds were apparent upon FLIM measurements (Fig. 2A). Average fluorescence lifetime of samples examined at 460 ± 30 nm increased from week 1 (1.4 ± 0.09 ns) to week 7 (2.2 ± 0.14 ns). The change in lifetime values was significant between all time points except between weeks 1 and 3 (Fig. 2B). The distribution of the lifetime histogram values became progressively narrower (full-width-at-half-maximum of 0.47 ± 0.1 ns in week 1 vs. 0.11 ± 0.1 ns in week 7) with increased culture time in chondrogenic conditions. These data suggest greater homogeneity of ECM content relating to collagen composition and associated collagen cross-links within each scaffold over prolonged culture (Fig. 2B). Similar trends were observed for both spectral ranges investigated (377 and 460 nm center wavelengths).

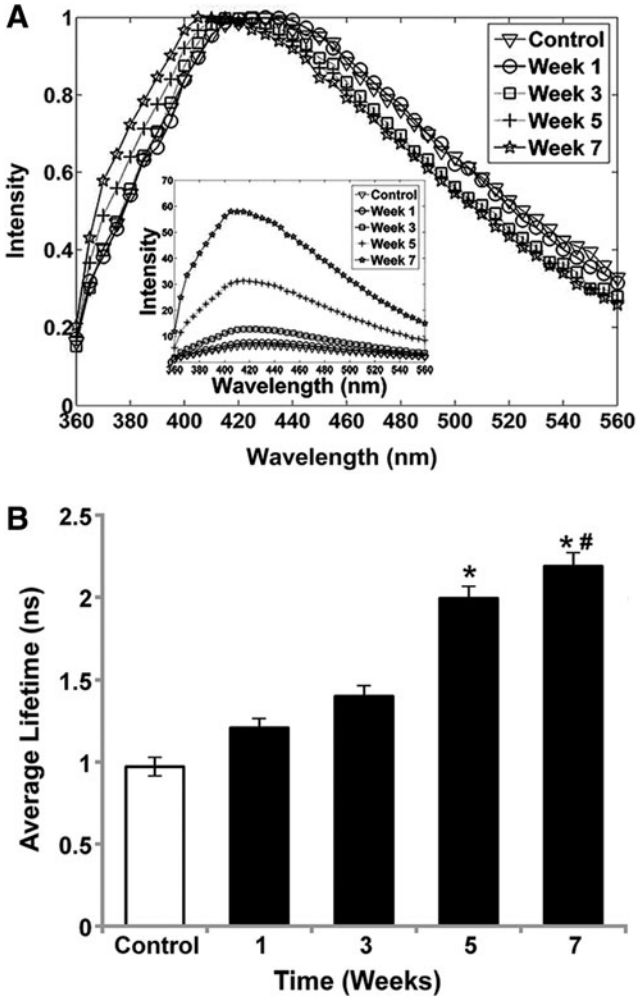

FIG. 1. **(A)** Normalized average fluorescence emission spectrum of chondrogenic samples retrieved for each time point (weeks 1, 3, 5, and 7) and control for comparison. Inset represents non-normalized emission spectra of the same samples. The spectra of all samples were averaged at each time point. **(B)** Average fluorescence lifetime averaged over all samples for each time point from TR-LIFS measurements (wavelength range 400–440 nm). The control value was obtained by averaging measurements of control samples for all time points. Data represent mean ± standard error of the mean (SEM) ($n = 4$, $^*p < 0.05$ vs. control, $^{\#}p < 0.05$ vs. week 3).

Ultrasound backscatter microscopy

We detected a significant difference in ultrasound attenuation between control and chondrogenic samples (Fig. 3),

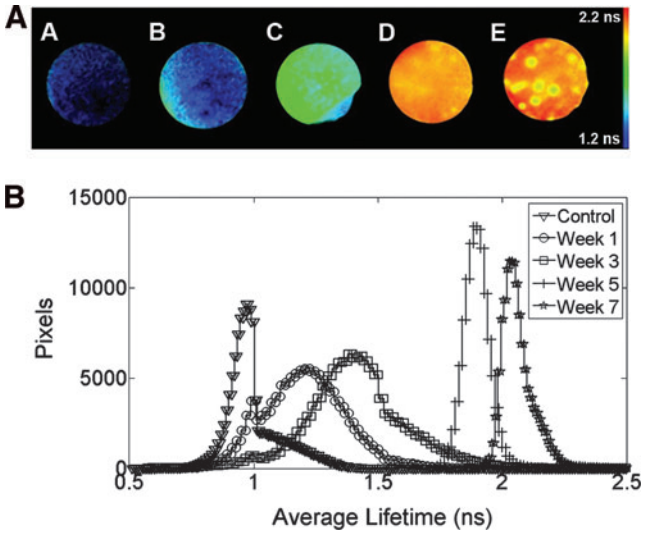

FIG. 2. **(A)** Representative average fluorescence lifetime images from fluorescence lifetime imaging microscopy measurements: (A) control sample and scaffolds cultured in chondrogenic conditions for (B) 1, (C) 3, (D) 5, and (E) 7 weeks. **(B)** Average fluorescence lifetime histogram of chondrogenic samples for each time point and control samples over 7 weeks ($n = 4$ for each week). Color images available online at www.liebertonline.com/tec.

with samples cultured in chondrogenic conditions exhibiting increasing attenuation with culture time. UBM images reconstructed the cross section of control scaffolds (Fig. 3A–C) and scaffolds in chondrogenic media (Fig. 3D–F) over 5 weeks. We were unable to collect UBM data at week 7 due to damage of the ultrasound transducer. While control scaffolds retained their original morphology, scaffolds maintained in chondrogenic conditions exhibited a pronounced curvature during the culture period, likely a function of cellular contraction, ECM deposition, and substrate remodeling. In agreement with these observations, ultrasound attenuation increased over time in chondrogenic samples, suggestive of increased matrix deposition. The signal of the chondrogenic group attenuated at a faster rate compared to that of the control group, as demonstrated by a plot of normalized intensity of the envelope of ultrasound signals as a function of sample depth (Fig. 3G). There were no significant changes for the attenuation of the control group over 5 weeks (Fig. 3H).

Histological characterization of tissue constructs

PSR staining confirmed progressive increases in collagen content, observed as any nonblack region, within chondrogenic constructs. Staining was most pronounced at week 7 in chondrogenic constructs (Fig. 4A) with increasing collagen deposition observed over longer culture durations, whereas control samples had no observable collagen (Fig. 4A, lower left inset). Upon quantification of total collagen content as a

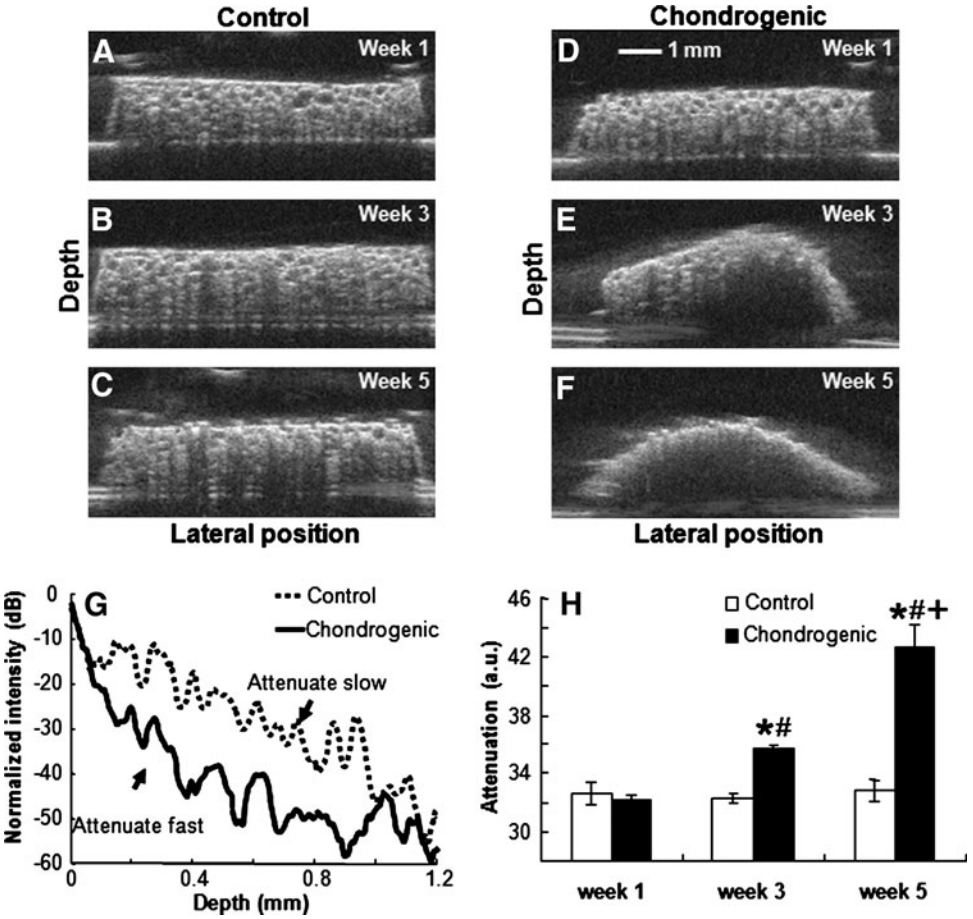

FIG. 3. Ultrasound backscatter microscopy images of **(A–C)** control scaffolds and **(D–F)** scaffolds cultured in chondrogenic conditions from week 1, 3, or 5 (top to bottom); **(G)** Changes in normalized intensity of the envelope of ultrasound signals as a function of sample depth; **(H)** changes in attenuation. Data are mean ± SEM from week 1 to 5 ($^{*}p < 0.05$ vs. control sample at the same time point, $^{\#}p < 0.05$ vs. week 1, $^{+}p < 0.05$ vs. weeks 1 and 3).

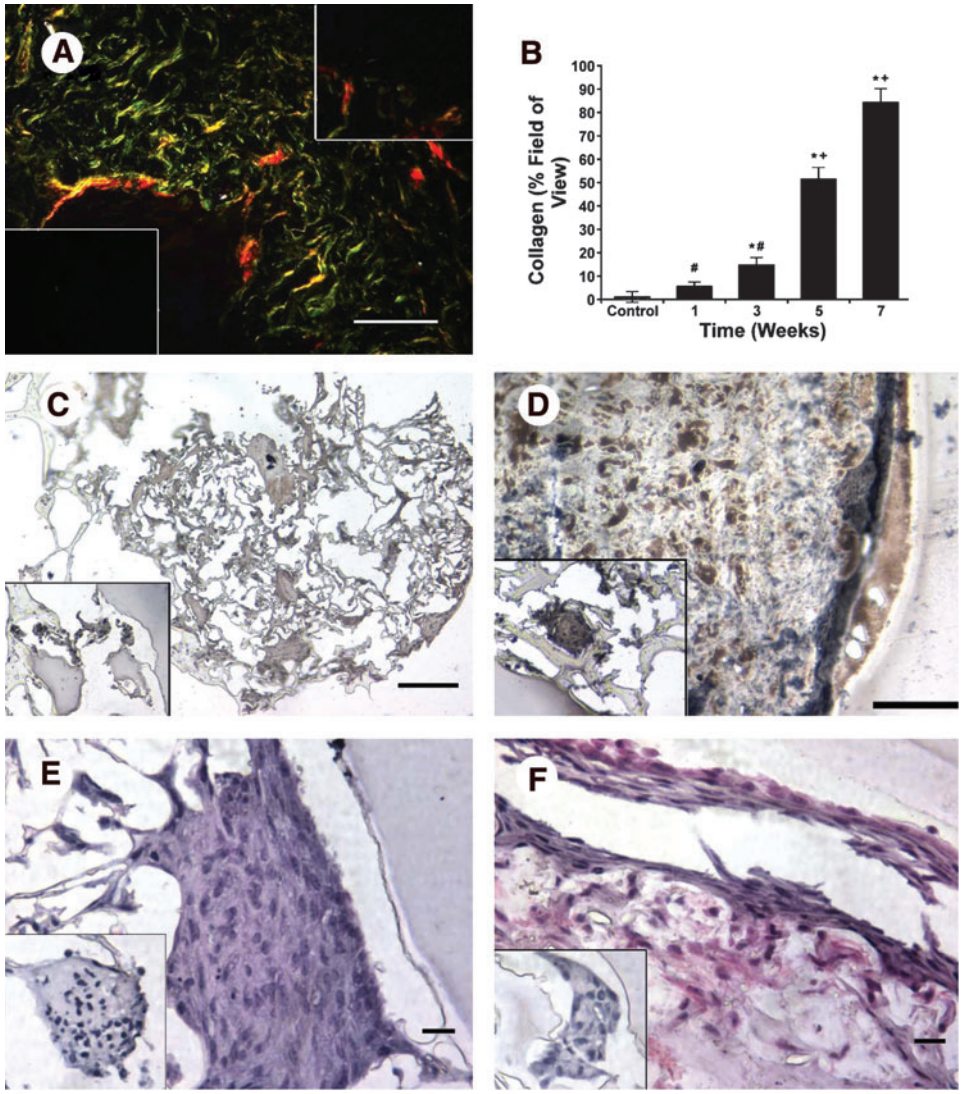

FIG. 4. Biochemical staining for total collagen, collagen type II, and glycosaminoglycans. **(A)** Picrosirius red (PSR) staining of scaffolds cultured in chondrogenic conditions for 7 weeks and observed at 100× magnification; scale bar represents 100 μm. Inset in upper right is PSR staining at 3 weeks in chondrogenic conditions, whereas inset in lower left is staining of construct in maintenance media after 7 weeks. **(B)** Quantification of collagen content as determined by PSR staining over 7 weeks; $^{*}p < 0.05$ vs. control, $^{\#}p < 0.05$ vs. weeks 5 and 7, $^{+}p < 0.05$ vs. all weeks). IHC for collagen type II after 3 **(C)** and 7 **(D)** weeks on construct in chondrogenic conditions; insets are constructs cultured in maintenance media for the same duration. Image shown at 10× magnification; scale bar is 200 μm. Safranin-O stain of constructs in chondrogenic media after 3 **(E)** and 7 **(F)** weeks. Insets are constructs cultured in maintenance media for the same duration. Images shown at 40× magnification; scale bar is 25 μm. Color images available online at www.liebertonline.com/tec.

function of sample coverage (Fig. 4B), we observed a significant difference between chondrogenic and control samples at weeks 5 and 7, yet no differences were apparent at weeks 1 or 3. Immunohistochemical staining for type II collagen in chondrogenic samples revealed minimal protein deposition (denoted as brown staining) after 3 weeks (Fig. 4C), yet staining was appreciably more extensive at week 7 (Fig. 4D). We failed to detect positive staining in control samples cultured in maintenance media for any time point. Staining for collagen type II confirmed diffuse protein distribution within the sample by week 7, with a noticeably larger amount around the edges of the scaffold. Safranin-O staining for GAG deposition revealed visible staining after 7 weeks of culture in samples maintained in chondrogenic conditions (Fig. 4F), but little GAG was evident after 3 weeks of culture (Fig. 4E), similar to type II collagen staining.

Cellularity and compressive testing of cell-seeded scaffolds

Scaffolds maintained in chondrogenic media exhibited greater DNA content throughout the 7-week study (Fig. 5A), with significant increases evident at weeks 1 and 3 compared to scaffolds in maintenance media. The increased cellularity in chondrogenic constructs likely resulted in early reductions in scaffold stiffness due to enzymatic degradation. However, we detected a stepwise increase in compressive modulus for samples in chondrogenic conditions over time (Fig. 5B), likely due to collagen II deposition by eASCs undergoing chondrogenic differentiation. Samples maintained in maintenance media exhibited a decrease in compressive modulus over the culture period. The reduction in scaffold stiffness likely results from minimal collagen deposition, as suggested by PSR and IHC, and scaffold digestion due to early cellular proliferation and increased acidic byproducts of anaerobic cellular metabolism by cells deprived of sufficient nutrients.

Relationships between fluorescence parameters, collagen content, and mechanical properties

A linear regression (Fig. 6) for all time points (weeks 1, 3, 5, and 7) revealed a significant correlation of the fluorescence intensity versus the compressive modulus ($R^2 = 0.998$, $p < 0.05$) and total collagen content vs. fluorescence intensity ($R^2 = 0.981$, $p < 0.05$).

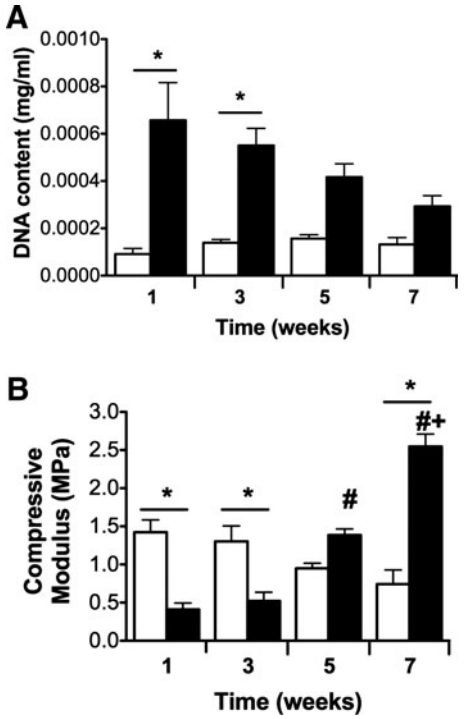

FIG. 5. **(A)** DNA content and **(B)** compressive moduli of cell-seeded constructs over time. Data are mean ± SEM ($n = 4$, $^{*}p < 0.05$ vs. control sample at the same time point, $^{\#}p < 0.05$ vs. weeks 1 and 3, $^{+}p < 0.05$ vs. weeks 1, 3, and 5). Control samples are open bars; chondrogenic samples are filled bars.

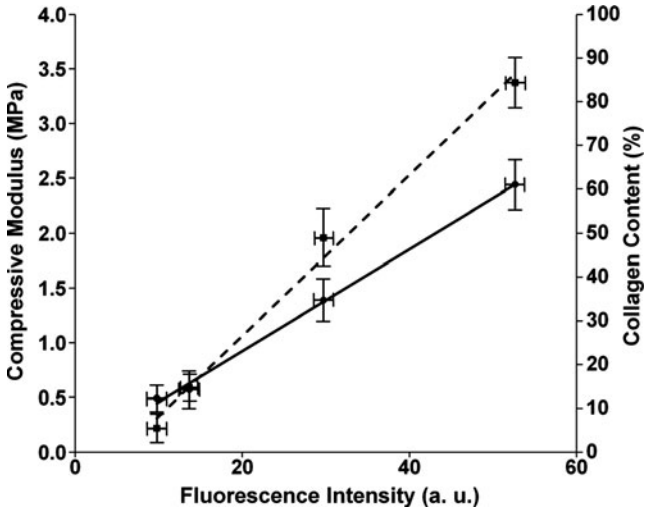

FIG. 6. Linear regression of fluorescence intensity versus compressive modulus of chondrogenic samples ($R^2 = 0.998$, $p < 0.05$) and versus total collagen content of chondrogenic samples ($R^2 = 0.981$, $p < 0.05$). Square markers and dashed line correspond to collagen content (right) y-axis, whereas circular markers and solid line corresponds to compressive modulus (left) y-axis.

Discussion

The results of this study suggest that optical imaging and spectroscopic modalities can be used to monitor bioengineered tissue formation *in vitro*. The three tissue characterization techniques (TRFS, FLIM, and UBM) utilized herein successfully detected changes in ECM content during chondrogenic differentiation of eASC on a 3D matrix that correlated strongly with standard biochemical and mechanical assays. Although this study was directed toward monitoring chondrogenic tissue maturation, these data demonstrate the feasibility of this approach for widespread application toward engineering other tissues including bone, vascular grafts, and soft tissue.

Upon appropriate stimulation, multipotent eASCs can be induced toward the chondrogenic[17] and other tissue lineages.[26,34] Chondrogenic differentiation is associated with expression of collagen, mostly type II, and GAGs,[22,24] thereby providing a target for optical detection. Collagen cross-links are responsible for collagen's strong autofluorescence,[35] and cross-linked collagen comprises the majority of articular cartilage ECM proteins, which increase rapidly during cartilage maturation,[23,24] and plateau once cartilage has reached maturity.[24] Previous studies report that increases in collagen cross-linking, achieved by the addition of advanced glycation end products, translate to increases in cartilage stiffness.[36] Similar increases in collagen cross-links, as well as total collagen, have been reported with the addition of TGF-β2 to chondrocytes in alginate beads,[37] and each of these processes occur over increased culture duration and construct aging. In addition, collagen cross-links represent a critical contributor to the mechanical properties of cartilage,[38] thereby providing a link between ECM content and stiffness. These data demonstrate increased collagen deposition with prolonged culture for constructs in chondrogenic conditions, and these findings are consistent with progenitor cells differentiating along a chondrogenic pathway. Further, these results are correlated with fluorescence measurements that demonstrate a continuous increase of fluorescence intensity (Fig. 1a) over the entire culture period. This observation suggests a linear relationship between the progressive increase in the amount of collagen cross-links formed in the tissue construct and the fluorescence intensity values. The time-resolved derived fluorescence parameters (i.e., lifetime) indicate that the type of fluorescent species produced during differentiation reaches a steady-state configuration and distribution within construct between week 5 and 7 of differentiation. This is demonstrated by both the nonsignificant increase of fluorescence lifetime values (Fig. 1b) and the narrow distribution of the lifetime histogram values (Fig. 2b) at weeks 5 and 7. Further, the increasing observance of cross-links correlated with increases in fluorescence intensity, average fluorescence lifetime, and stiffness of the construct (Fig. 6).

While TRFS and FLIM are characterized by distinct detection methods, including optical pathways, light delivery systems, and fluence rate reaching the sample, the fluorescence decay characteristics of tissue constructs retrieved with both techniques were consistent. Both modalities revealed significant increases in average fluorescence lifetime values as a function of time, ranging from ~ 1 ns in control samples to ~ 2.2 ns in chondrogenically induced samples after 7 weeks. This underscores the advantage of time-resolved fluorescence methods that allow for the characterization of tissue fluorescence emission independent of the excitation intensity and light excitation-collection geometries.

However, while TRFS enables the interrogation of both sample fluorescence spectrum profile and lifetime values along the emission spectrum, FLIM facilitates an assessment of tissue heterogeneity via formation of a fluorescence lifetime image. Consequently, these modalities complement each other to yield a rapid and more complete characterization of the fluorescent sample. Given the biochemical content of cartilage tissue constructs, the most likely autofluorescent biomolecules in these constructs are the enzyme cofactor NAD(P)H in cell and the constituents of the ECM (e.g., collagen II and its cross-links, and GAG). The fluorescence emission of these biological fluorophores was previously studied and reported.[7–10,39] Upon UV excitation around 337 nm, NAD(P)H exhibits a peak emission centered between 440 and 460 nm with a lifetime that ranges from ~0.5 ns (free form) to 2–3 ns (protein-bounded forms), whereas mature collagen type II presents a blue-shifted peak emission at about 380–390 nm with and a longer lifetimes over 3 ns. Collagen fluorescence emission peak, bandwidth, and band-shape change with excitation wavelength. The 3-hydroxypyridinium cross-link or pyridinoline (peak absorption at 325 nm) presents a peak fluorescence emission around 390 nm and was identified as an abundant component of cartilage collagen.[40] Thus, this cross-link is most likely to dominate the fluorescence of mature collagen type II. While GAG demonstrated a peak fluorescence emission at about 390 nm, similar to collagen type II at 337 nm, GAG emission measured in tissue extracts for the same excitation fluence rate was found at least two times weaker than that of collagen type II (data unpublished). This suggests that the collagen emission characteristics are most likely to dominate the overall fluorescence emission when both collagen and GAG molecules are present. Current TRFS and FLIM results obtained for cartilage constructs suggest that for weeks 1–3 the weak and short-lived fluorescence that peaks at ~440 nm is mainly generated by NAD(P)H in cells. The blue-shifted increased fluorescence intensity and longer lifetime values observed after week 3 suggests that collagen and its cross-links began to contribute to cartilage construct fluorescence.

As shown in these studies, these fluorescence-based techniques can effectively characterize ECM content, which is of critical importance for evaluating the development of functional tissue constructs. Along with other optical methods such us Raman spectroscopy,[41,42] we anticipate that fluorescence techniques will provide a new dimension for the nondestructive evaluation of bioengineered tissue within a host of culture environments (e.g., tissue culture, small- and large-scale bioreactors). The capacity to frequently and reliably monitor ECM composition and cross-link formation will facilitate customized maintenance of each tissue construct—an important opportunity in light of the donor-to-donor variability in cellular responsiveness to lineage-specific cues. Additionally, optical methods offer high resolution (except in depth), high specificity, and sensitivity to biological changes, while also enabling multiple measurements over a short period of time without tissue damage.

We determined that UBM measurements successfully complemented the optical methods by providing morphological information of the cross section of the sample and permitting construct sampling at greater penetration depth without sacrificing any tissue. In its current configuration, UBM can reach a penetration depth of 5–6 mm, which is an order of magnitude deeper than attainable for the optical techniques applied here (<250 μm). The analysis of the ultrasound RF signals facilitates not only a direct observation of the sample but also functional information.

While the current study produced very promising results, it also identified a number of challenges with regard to routine assessment of larger tissue constructs. Most notably, the optical methods described here rely on excitation in the near UV range, which results in limited depth resolution (200–250 μm at 337 nm). While this may be ameliorated to a degree through the use of two-photon excitation, this method requires complex and expensive instrumentation that may limit its applicability for routine monitoring of engineered tissue constructs. The development of improved techniques to reliably and reproducibly detect autofluorescent moieties at greater depths merits further investigation. In addition, the static seeding of eASC on polymeric scaffolds results in heterogeneous distribution of cells,[43] and this lack of homogeneity within a single scaffold may alter the correlation between optical and biochemical data.

Although equine cells were used in this study due to their ready availability and accelerated proliferative potential, the results of this study have relevance to human medicine. Indeed, our results are in agreement with previous studies that have successfully applied optical techniques, such as fluorescence lifetime contrast, to monitor the differentiation of multipotent human progenitor cells toward the osteogenic lineage.[12] Moreover, we confirmed that chondrogenically induced eASC demonstrate an increase in collagen (particularly type II) expression over time, and this is in agreement with previous studies.[44,45] As mechanisms of differentiation are highly conserved between mammalian stem and progenitor cells, it is expected that the application of optical techniques toward constructs seeded with human cells will yield similar results.

Conclusion

The application of optical and ultrasonic techniques offers a novel method for monitoring the rate and quality of tissue maturation by following a construct's chemical composition, structure, and mechanical properties in a nondestructive and noninvasive manner. This approach may have a profound benefit in the *ex vivo* growth of engineered tissues where conventional analysis techniques are destructive, require comparatively large amounts of the tissue construct, and incur significant additional resources. Moreover, any single modality examined in this study demonstrated the ability to discriminate between changes in constructs maintained in growth or chondrogenic environments, yet the combination of the three modalities provides additional information that may enable accurate discrimination complex engineered tissues.

Acknowledgments

This study was funded in part by NIH (Grant nos. UL1-RR024146, R25-GM56765, and R01-HL067377-05A1), The Hartwell Foundation, the Howard Hughes Medical Institute Med into Grad Initiative (Grant no. 56005706), and the Training program in Basic and Translational Cardiovascular Science (Grant no. HL086350-01A1). The authors thank

Drs. Larry Galuppo and Martin Vidal of the UC Davis School of Veterinary Medicine for providing equine tissues, Dr. Kirk Shung of the University of Southern California for providing the ultrasonic transducer used in the study, and Dr. Kyriacos Athanasiou for valuable discussions.

Disclosure Statement

No competing financial interests exist.

References

1. Langer, R., and Vacanti, J.P. Tissue engineering. Science **260,** 920, 1993.
2. Atala, A. Engineering organs. Curr Opin Biotechnol **20,** 575, 2009.
3. Akhtar, R., Schwarzer, N., Sherratt, M.J., Watson, R.E., Graham, H.K., Trafford, A.W., Mummery, P.M., and Derby, B. Nanoindentation of histological specimens: mapping the elastic properties of soft tissues. J Mater Res **24,** 638, 2009.
4. Ateshian, G.A., and Ricken, T. Multigenerational interstitial growth of biological tissues. Biomech Model Mechanobiol **9,** 689, 2010.
5. Andersson-Engels, S., Johansson, J., Stenram, U., Svanberg, K., and Svanberg, S. Time-resolved laser-induced fluorescence spectroscopy for enhanced demarcation of human atherosclerotic plaques. J Photochem Photobiol B **4,** 363, 1990.
6. Elson, D.S., Galletly, N., Talbot, C., Requejo-Isidro, J., McGinty, J., Dunsby, C., Lanigan, P.M.P., Munro, I., Benninger, R.K.P., De Beule, P., Auksorius, E., Hegyi, L., Sandison, A., Wallace, A., Soutter, P., Neil, M.A.A., Lever, J., Stamp, G.W., and French, P.M.W. Multidimensional Fluorescence Imaging Applied to Biological Tissue. New York: Springer Science, 2006.
7. Richards-Kortum, R., and Sevick-Muraca, E. Quantitative optical spectroscopy for tissue diagnosis. Annu Rev Phys Chem **47,** 555, 1996.
8. Marcu, L., Fishbein, M.C., Maarek, J.M., and Grundfest, W.S. Discrimination of human coronary artery atherosclerotic lipid-rich lesions by time-resolved laser-induced fluorescence spectroscopy. Arterioscler Thromb Vasc Biol **21,** 1244, 2001.
9. Georgakoudi, I., Jacobson, B.C., Muller, M.G., Sheets, E.E., Badizadegan, K., Carr-Locke, D.L., Crum, C.P., Boone, C.W., Dasari, R.R., Van Dam, J., and Feld, M.S. NAD(P)H and collagen as *in vivo* quantitative fluorescent biomarkers of epithelial precancerous changes. Cancer Res **62,** 682, 2002.
10. Wagnieres, G.A., Star, W.M., and Wilson, B.C. *In vivo* fluorescence spectroscopy and imaging for oncological applications. Photochem Photobiol **68,** 603, 1998.
11. Farwell, D.G., Meier, J.D., Park, J., Sun, Y., Coffman, H., Poirier, B., Phipps, J., Tinling, S., Enepekides, D.J., and Marcu, L. Time-resolved fluorescence spectroscopy as a diagnostic technique of oral carcinoma: validation in the hamster buccal pouch model. Arch Otolaryngol Head Neck Surg **136,** 126, 2010.
12. Ashjian, P., Elbarbary, A., Zuk, P., DeUgarte, D.A., Benhaim, P., and Hedrick, M.H. Noninvasive *in situ* evaluation of osteogenic differentiation by time-resolved laser-induced fluorescence spectroscopy. Tissue Eng **10,** 411, 2004.
13. Huang, A.H., Farrell, M.J., and Mauck, R.L. Mechanics and mechanobiology of mesenchymal stem cell-based engineered cartilage. J Biomech **43,** 128, 2010.
14. Lu, H.H., and Jiang, J. Interface tissue engineering and the formulation of multiple-tissue systems. Adv Biochem Eng Biotechnol **102,** 91, 2006.
15. Kempson, G.E., Muir, H., Swanson, S.A., and Freeman, M.A. Correlations between stiffness and the chemical constituents of cartilage on the human femoral head. Biochim Biophys Acta **215,** 70, 1970.
16. Responte, D.J., Natoli, R.M., and Athanasiou, K.A. Collagens of articular cartilage: structure, function, and importance in tissue engineering. Crit Rev Biomed Eng **35,** 363, 2007.
17. Kisiday, J.D., Kopesky, P.W., Evans, C.H., Grodzinsky, A.J., McIlwraith, C.W., and Frisbie, D.D. Evaluation of adult equine bone marrow- and adipose-derived progenitor cell chondrogenesis in hydrogel cultures. J Orthop Res **26,** 322, 2008.
18. Castillo, A.B., and Jacobs, C.R. Mesenchymal stem cell mechanobiology. Curr Osteoporos Rep **8,** 98, 2010.
19. Reed, S.A., and Johnson, S.E. Equine umbilical cord blood contains a population of stem cells that express Oct4 and differentiate into mesodermal and endodermal cell types. J Cell Physiol **215,** 329, 2008.
20. Lu, J.M., Zhou, Z.Y., Zhang, X.R., Li, X.L., Wang, H.F., and Song, X.J. A preliminary study of mesenchymal stem cell-like cells derived from murine corneal stroma. Graefes Arch Clin Exp Ophthalmol **248,** 1279, 2010.
21. Patel, J., Gudehithlu, K.P., Dunea, G., Arruda, J.A., and Singh, A.K. Foreign body-induced granulation tissue is a source of adult stem cells. Transl Res **155,** 191, 2010.
22. van der Harst, M.R., Brama, P.A., van de Lest, C.H., Kiers, G.H., DeGroot, J., and van Weeren, P.R. An integral biochemical analysis of the main constituents of articular cartilage, subchondral and trabecular bone. Osteoarthritis Cartilage **12,** 752, 2004.
23. Williamson, A.K., Chen, A.C., Masuda, K., Thonar, E.J., and Sah, R.L. Tensile mechanical properties of bovine articular cartilage: variations with growth and relationships to collagen network components. J Orthop Res **21,** 872, 2003.
24. Julkunen, P., Harjula, T., Iivarinen, J., Marjanen, J., Seppanen, K., Narhi, T., Arokoski, J., Lammi, M.J., Brama, P.A., Jurvelin, J.S., and Helminen, H.J. Biomechanical, biochemical and structural correlations in immature and mature rabbit articular cartilage. Osteoarthritis Cartilage **17,** 1628, 2009.
25. Kollias, N., Gillies, R., Moran, M., Kochevar, I.E., and Anderson, R.R. Endogenous skin fluorescence includes bands that may serve as quantitative markers of aging and photoaging. J Invest Dermatol **111,** 776, 1998.
26. Cheung, W.K., Working, D.M., Galuppo, L.D., and Leach, J.K. Osteogenic comparison of expanded and uncultured adipose stromal cells. Cytotherapy **12,** 554, 2010.
27. Toupadakis, C.A., Wong, A., Genetos, D.C., Cheung, W.K., Borjesson, D.L., Ferraro, G.L., Galuppo, L.D., Leach, J.K., Owens, S.D., and Yellowley, C.E. Comparison of the osteogenic potential of equine mesenchymal stem cells from bone marrow, adipose tissue, umbilical cord blood, and umbilical cord tissue. Am J Vet Res **71,** 1237, 2010.
28. Davis, H.E., Rao, R.R., He, J., and Leach, J.K. Biomimetic scaffolds fabricated from apatite-coated polymer microspheres. J Biomed Mater Res **90,** 1021, 2009.
29. Jo, J.A., Fang, Q., and Marcu, L. Ultrafast method for the analysis of fluorescence lifetime imaging microscopy data based on the Laguerre expansion technique. IEEE J Quantum Electron **11,** 835, 2005.
30. Jo, J.A., Fang, Q., Papaioannou, T., Baker, J.D., Dorafshar, A.H., Reil, T., Qiao, J.H., Fishbein, M.C., Freischlag, J.A., and Marcu, L. Laguerre-based method for analysis of time-resolved

fluorescence data: application to *in-vivo* characterization and diagnosis of atherosclerotic lesions. J Biomed Opt **11,** 021004, 2006.
31. Elson, D.S., Jo, J.A., and Marcu, L. Miniaturized side-viewing imaging probe for fluorescence lifetime imaging (FLIM): validation with fluorescence dyes, tissue structural proteins and tissue specimens. New J Phys **9,** 127, 2007.
32. Sun, Y., Park, J., Stephens, D.N., Jo, J.A., Sun, L., Cannata, J.M., Saroufeem, R.M., Shung, K.K., and Marcu, L. Development of a dual-modal tissue diagnostic system combining time-resolved fluorescence spectroscopy and ultrasonic backscatter microscopy. Rev Sci Instrum **80,** 065104, 2009.
33. He, J., Genetos, D.C., Yellowley, C.E., and Leach, J.K. Oxygen tension differentially influences osteogenic differentiation of human adipose stem cells in 2D and 3D cultures. J Cell Biochem **110,** 87, 2010.
34. Vidal, M.A., Kilroy, G.E., Lopez, M.J., Johnson, J.R., Moore, R.M., and Gimble, J.M. Characterization of equine adipose tissue-derived stromal cells: adipogenic and osteogenic capacity and comparison with bone marrow-derived mesenchymal stromal cells. Vet Surg **36,** 613, 2007.
35. Young, A.R. Chromophores in human skin. Phys Med Biol **42,** 789, 1997.
36. Verzijl, N., DeGroot, J., Zaken, C.B., Braun-Benjamin, O., Maroudas, A., Bank, R.A., Mizrahi, J., Schalkwijk, C.G., Thorpe, S.R., Baynes, J.W., Bijlsma, J.W.J., Lafeber, F.P.J.G., and TeKoppele, J.M. Crosslinking by advanced glycation end products increases the stiffness of the collagen network in human articular cartilage: a possible mechanism through which age is a risk factor for osteoarthritis. Arthritis Rheum **46,** 114, 2002.
37. Bastiaansen-Jenniskens, Y.M., Koevoet, W., De Bart, A.C., Zuurmond, A.M., Bank, R.A., Verhaar, J.A., DeGroot, J., and van Osch, G.J. TGFbeta affects collagen cross-linking independent of chondrocyte phenotype but strongly depending on physical environment. Tissue Eng Part A **14,** 1059, 2008.
38. Williamson, A.K., Chen, A.C., and Sah, R.L. Compressive properties and function-composition relationships of developing bovine articular cartilage. J Orthop Res **19,** 1113, 2001.
39. Marcu, L., Cohen, D., Maarek, J.M., and Grundfest, W.S. Characterization of type I, II, III, IV, and V collagens by time-resolved laser-induced fluorescence spectroscopy. Optical biopsy III, SPIE Proceedings, 2000, pp. 93–101.
40. Wu, J.J., and Eyre, D.R. Identification of hydroxypyridinium cross-linking sites in type II collagen of bovine articular cartilage. Biochemistry **23,** 1850, 1984.
41. Pully, V.V., Lenferink, A., van Manen, H.J., Subramaniam, V., van Blitterswijk, C.A., and Otto, C. Microbioreactors for Raman microscopy of stromal cell differentiation. Anal Chem **82,** 1844, 2010.
42. Boyd, A.R., Burke, G.A., and Meenan, B.J. Monitoring cellular behaviour using Raman spectroscopy for tissue engineering and regenerative medicine applications. J Mater Sci Mater Med **21,** 2317, 2010.
43. Wendt, D., Marsano, A., Jakob, M., Heberer, M., and Martin, I. Oscillating perfusion of cell suspensions through three-dimensional scaffolds enhances cell seeding efficiency and uniformity. Biotechnol Bioeng **84,** 205, 2003.
44. Giovannini, S., Brehm, W., Mainil-Varlet, P., and Nesic, D. Multilineage differentiation potential of equine blood-derived fibroblast-like cells. Differentiation **76,** 118, 2008.
45. Koerner, J., Nesic, D., Romero, J.D., Brehm, W., Mainil-Varlet, P., and Grogan, S.P. Equine peripheral blood-derived progenitors in comparison to bone marrow-derived mesenchymal stem cells. Stem Cells **24,** 1613, 2006.

Address correspondence to:
Laura Marcu, Ph.D.
Department of Biomedical Engineering
University of California, Davis
451 Health Sciences Drive, GBSF 2513
Davis, CA 95616

E-mail: lmarcu@ucdavis.edu

J. Kent Leach, Ph.D.
Department of Biomedical Engineering
University of California, Davis
451 Health Sciences Drive, GBSF 3321
Davis, CA 95616

E-mail: jkleach@ucdavis.edu

Received: June 22, 2010
Accepted: December 17, 2010
Online Publication Date: February 4, 2011